frontiers | Frontiers in Environmental Science

TYPE Original Research
PUBLISHED 01 September 2022
DOI 10.3389/fenvs.2022.978559

OPEN ACCESS

EDITED BY
Kun-Yi Andrew Lin,
National Chung Hsing University, Taiwan

REVIEWED BY
Titus Egbosiuba,
Chukwuemeka Odumegwu Ojukwu University, Nigeria
Mi Yan,
Zhejiang University of Technology, China

*CORRESPONDENCE
Zongwen Zhao,
zhaozongw@126.com

SPECIALTY SECTION
This article was submitted to Toxicology, Pollution and the Environment, a section of the journal Frontiers in Environmental Science

RECEIVED 26 June 2022
ACCEPTED 11 August 2022
PUBLISHED 01 September 2022

CITATION
Wang Z, Jie F, Li W, Zhao Z, Niu F, Zhu J, Qin W and Zhou K (2022), Investigation of the occurrence characteristics of organic components in high-sulfur waste residues (HSWR).
Front. Environ. Sci. 10:978559.
doi: 10.3389/fenvs.2022.978559

Investigation of the occurrence characteristics of organic components in high-sulfur waste residues (HSWR)

Zhongbing Wang[1,2,3], Fanghui Jie[4], Weiqi Li[2,5], Zongwen Zhao[1,2,3]*, Fei Niu[2,5], Junqiang Zhu[2,5], Weining Qin[2,5] and Kai Zhou[2,5]

[1]School of Metallurgy and Environment, Central South University, Changsha, Hunan, China, [2]Dongjiang Environmental Co., Ltd., Shenzhen, Guangdong, China, [3]Postdoctoral Mobile Station of Central South University, Changsha, Hunan, China, [4]Jiangxi Ganchang Evaluation and Testing Technology Consulting Co., Ltd., Nanchang, Jiangxi, China, [5]Guangdong Provincial Key Laboratory of R&D for Resource Utilization and Deep Treatment of Hazardous Waste Liquid, Shenzhen, Guangdong, China

High-sulfur waste residues (HSWR) is a typical byproduct produced in the printing and dyeing industry that has hazardous properties, such as flammability and reactivity, etc. It is of great significance for the directional and harmless treatment of waste residues in the later stage on the research in-depth of the occurrence characteristics of each component in HSWR. In this paper, the combinatorial analysis method is employed to perform in-depth research on the phase composition, surface chemical situation of element, and the occurrence state of functional groups of the waste residue from multiple perspectives. The results show that the organic and inorganic components in HSWR are intricately interwoven, and exhibit significant thermal instability at high temperatures, with a maximum weight less of 86.66%. Carbon mainly exists in the states of C-H/C-OH/C-C, C-O/C-NH_2, and C=O/C-N/C-S/CH_x and constitutes the main chain of the carboxylic ring. Sulfur mainly occurs in three forms, namely, amorphous aggregated sulfur, sulfur-containing inorganic salts such as sulfate, and nitrogen-heterocyclic organic compounds containing sulfhydryl groups and methyl sulfur groups. These organic compounds constitute branch chains of the organic phase, and combine with metal cations through hydroxyl or carboxyl groups, and deposit on the surface of inorganic agglomerated sulfur. This wrapping structure increases the stability of volatile compounds in the slag and increases the difficulty of sulfur and chlorine removal. These findings provide a material basis for the later development of safe and effective HSWR disposal techniques.

KEYWORDS

hSWR, sulfur, organic matter, occurrence characteristics, harmless treatment

1 Introduction

Fine chemicals are one of the most dynamic emerging fields in the chemical industry today, they are also an important part of many new materials, covering more than 40 multiple industries and categories such as textile printing and dyeing, catalysts, electronic chemicals and materials, functional polymer materials, Biochemical, etc. (Vásquez-Céspedes et al., 2021). With the rapid development of the global economy and the rise of various high-tech chemical industries, the consumption and development of chemical products have greatly increased, which is also accompanied by the discharge of numerous of pollutants (Dong et al., 2018; Huang et al., 2018). According to China's 2020 environmental statistics report, the solid waste generated by the fine chemical industry accounts for 5% of the country's total emissions, which ranks fifth (Ciriminna et al., 2021). The solid waste generated by the fine chemical industry is basically included on the latest National Hazardous Waste List (2021 edition) of China. The safe and effective disposal of these solid wastes is important to the realization of green production in the fine chemical industry (Yao et al., 2019).

High-sulfur waste residue (HSWR) are a typical chemical waste residue, that is mainly derived from the pharmaceutical, pesticide, printing and dyeing industries (Zhang et al., 2017a). There are two main sources of HSWR: the first source consists of the unqualified products and intermediate products produced in production. Due to product quality requirements, unqualified products cannot be reused as secondary raw materials, and are usually treated as waste residues, while most of the intermediate products are converted from spent sulfur-containing catalysts, sulfuric acid and other materials. The second source consists of the waste residue and other harmful substances produced by filtration, rectification and other processes after the raw materials react in a reactor. Therefore, according to its source and process characteristics, the main characteristics of HSWR are detailed as follows: 1) Wide-ranging sources. There are obvious differences in the nature of wastes generated in different industries, resulting in insufficient mixed storage and disposal of such wastes. 2) Various forms. The large number of sources cause chemical waste residues to have liquid, colloidal, solid and other forms, and their colors are ever-changing. 3) Complex composition. The content of sulfur and chlorine is high; the occurrence phase is complex; and the organic and inorganic phases are mixed and embedded with each other. 4) High calorific value. The slag contains a certain organic phase, resulting in a high calorific value of the waste itself, which is prone to spontaneous combustion under certain conditions. 5) Low pH value and strong corrosiveness. Under certain conditions, HSWR easily reactes with water vapor and water in the air to generate acid gases such as SO_2, H_2S, and HCl. 6) HSWR has a strong pungent odor and toxicity (Zhao et al., 2020; Tceab and Asab, 2021). Development so far, dozens of desulfurization technologies have been reported worldwide. According to its development history, it can be divided into traditional desulfurization technologies, such as wet (Li et al., 2022), semidry (Liu et al., 2021), and dry desulfurization (Ding et al., 2019), and current mainstream technologies, such as gas-phase reduction and liquid-phase reduction (Raymundo-Pinero et al., 2000; Mentzen et al., 2010; Bejarano et al., 2001; Chambers and Trudinger, 1975; Kline et al., 1987; Tolmachev and Scherson, 1999). Although these technologies are widely employed in the raw coal treatment and waste tire disposal industry, they have obvious drawbacks. Basically, they are first burned and then adsorbed and solidified by sulfur-fixing/chlorine agents. However, for HSWR, because the sulfur content is much higher than that in raw coal and because the slag contains numerous of organic components, it is not suitable for the abovementioned technology to be treated. Presently, incineration and neutralization methods are mainly utilized in industry to dispose of HSWR. Incineration is divided into jet incineration and material mixing incineration according to the state of waste. The injection is mainly aimed at high-sulfur slag in the form of a liquid. Material mixing incineration is mainly aimed at solid or colloidal high-sulfur waste, generally, the maximum mixing ratio is controlled below 20%. The neutralization method is to carry out the acid-base neutralization reaction of high-sulfur waste and alkaline wastewater to form inorganic salts with low toxicity and corrosiveness. However, these methods have obvious shortcomings: the liquid flow rate of jet incineration cannot be too large, or a sudden increase in the concentration of pollutants in the flue gas can easily occur, and the exhaust gas is discharged beyond the standard. In addition, jet incineration is also likely to cause the liquid outside the furnace to burn, causing the risk of fire. The treatment capacity of material mixing incineration is extremely low; neutralization treatment will produce a large amount of industrial waste salt, which hinders secondary treatment. Based on the backwardness of the existing disposal technologies, the disposal amount of HSWR is substantially lower than its production amount, resulting in the storage of a large amount of HSWR in warehouses, which poses great safety and environmental hazard (Egbosiuba et al., 2020a). There is an urgent need to develop a safe treatment technology for HSWR to achieve harmlessness and reduction. The premise to reach this goal is to acquire a good knowledge of the occurrence characteristics of each component in HSWR, which has an important role in the development of HSWR harmless and reduction technology. However, many reports at home and abroad are more focused on the desulfurization process and mechanism. Tang et al. (2018) used molten salt pyrolysis to desulphurize high-sulfur waste tires *in situ*, so that organic sulfur was pyrolyzed into $^{\bullet}SH$, and formed metal sulfides with metals to achieve the purpose of solidifying sulfur and reducing the generation of H_2S. Liu et al. (2019) studied the effects of three kinds of industrial waste residues on the catalytic combustion of high-sulfur coal by comparison method. Zilberchmidt et al. (2004) deeply analyzed the feasibility of thermal treatment of high-sulfur coal wastes. There are very few reports on basic research on the occurrence characteristics of organic components in HSWR, resulting in generally unclear understanding of the basic properties of HSWR. Therefore, it is of great significance for the directional and harmless treatment of waste residues in the later stage on the research in-depth of the occurrence characteristics of each component in HSWR.

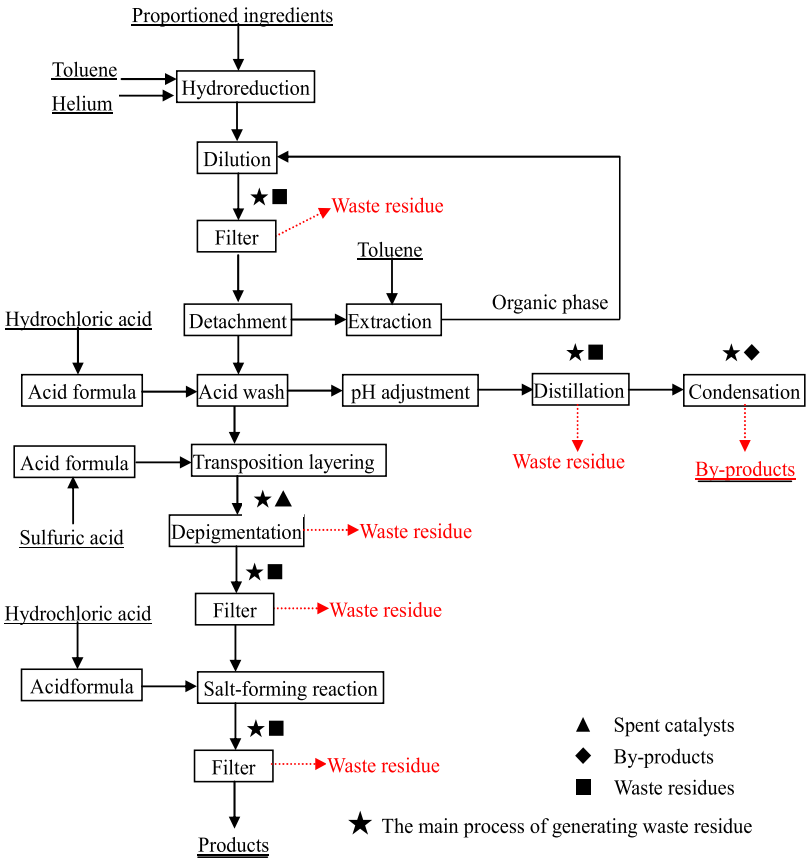

FIGURE 1
Production process of a paint in the printing and dyeing industry and the main process of waste residue generation.

In this paper, a typical HSWR is selected from the printing and dyeing industry as the research object. Composition quantitative analysis, elemental analysis (EA), thermogravimetric-differential scanning calorimetry (TG-DSC), X-ray diffraction (XRD), scanning electron microscopy-energy dispersive spectrometry (SEM-EDS), Fourier transform infrared spectrometry (FTIR), and X-ray photoelectron spectroscopy (XPS) were jointly utilized to analyze the composition and its occurrence. These findings contribute to the development of safe and efficient disposal techniques for HSWR.

2 Process description and analysis methods

2.1 Process description and waste residue source

Fine chemicals cover the production of hundreds of products, and different products have different characteristics and application fields, resulting in large differences in the corresponding production processes and main raw materials. However, in addition to the main raw materials required in production, most chemical products use a large amount of general-purpose catalysts, organic additives, hydrochloric acid, sulfuric acid, etc., in their production. After reduction, synthesis and rectification, etc., of these main raw materials and auxiliary raw materials, most of them are converted to main products and some of them are converted into impurities to the slag phase or converted to byproducts and spent catalysts. Figure 1 shows the production process of a coating in the printing and dyeing industry and the main process of waste residue generation. Notably, there are three main sources of HSWR: 1) waste residues from production, 2) spent catalysts, 3) byproducts generated during production.

2.2 Analytical method

2.2.1 Sample pretreatment

Before the analysis and characterization, HSWR used in the experiment was first baked in drying oven at temperature of

60°C–80°C for 5 h, due to the high moisture content of the original waste residue, and then ground into powder and stored in a sealed bag for later use. The purpose of low baking temperature is to reduce the loss of volatile or easily decomposed compounds in HSWR.

2.2.2 Composition analysis

The elements H, O, and N, S in the organic components of the waste residue were determined by EA (VarioELcube, Germany). The total nitrogen was analyzed by ultraviolet spectrophotometry (HJ/T346-2007). Sulfate was analyzed by the gravimetric method (GB/T 11899-1989). Chloride ions were determined by the silver nitrate titration method (GB/T 11896-1989). The total sulfur was analyzed by the determination method of total sulfur in coal (GB/T 214-2007). The total organic carbon and total carbon were analyzed by the high-temperature combustion—nondispersive infrared absorption method. The remaining elements were determined by ICP–AES (Egbosiuba et al., 2020b).

2.2.3 Characterization analysis

The comprehensive thermal behaviors of the HSWR at temperatures ranging from room temperature to 1,000°C were analyzed with a TG-DSC apparatus (NETZSCH STA 449C; NETZSCH Pumps North America LLC, Exton, PA) in argon flowing at a heating rate of 10°C/min. The phase evolution and structural features of the HSWR were identified by XRD (D/max2550 VB) + X with a Cu (40 kV, 300 mA) radiation source, steps of 10°/min for 2θ values ranging from 10° to 80° (Wang et al., 2021; Zhao et al., 2021; Egbosiuba et al., 2022). The micromorphology and element distribution were observed by scanning electron microscopy (SEM, TESCAN MIRA3 XMH and FEI Helios Nanolab 600i) equipped with an energy dispersive spectrometer (EDS, QUANTAX 400, Bruker) system (Egbosiuba et al., 2020c). FTIR data was collected in the range of 400–4,000 cm^{-1} using a BRUKER, VERTEX70 spectrometer at 4 cm^{-1} resolution using the KBr pellet technique. X-ray photoelectron spectroscopy (XPS) experiments were carried out on a Thermo Fisher Nexsa using an Al K-a X-ray source (1486.6 eV). All spectra were calibrated with graphitic carbon as the reference at a binding energy (BE) of 284.8 eV. For C1s, O1s, S2p, N1s, and Cl2p, the spectra were deconvolved with the subtraction of a linear background and with a Gaussian (80%)–Lorentzian (20%) mixed function (Wang et al., 2019; Wang et al., 2022).

TABLE 1 List of elemental compositions of HSWR.

No.	Element	(wt%)
1	Calorific value	3000 cal/g
2	Ca	0.010
3	Fe	0.075
4	Mg	0.021
5	Na	1.051
6	S	72.372
7	Cl	8.62
8	Si	0.009
9	P	< 0.005
10	Zn	< 0.005
11	Al	< 0.005
12	As	< 0.005
13	Sb	< 0.005
14	B	< 0.005
15	Ba	< 0.005
16	Ni	< 0.005
17	Hg	< 0.005
18	Ca	< 0.005
19	Cd	< 0.005
20	Pb	< 0.005
21	Cu	< 0.005
22	K	< 0.005
23	Co	< 0.005
24	Li	< 0.005
25	Cr	< 0.005

TABLE 2 Quantitative analysis of main elements and compounds in HSWR.

Component	(wt%)
Sulfate	2.36
Chloride	2.57
Total sulfur	72.37
Total organic carbon	5.96
Total nitrogen	2.58
Total hydrogen	0.66
Total oxygen	4.36

3 Results and discussions

3.1 Characterizations of the HSWR

3.1.1 Chemical compositions

The chemical compositions of the HSWR are presented in Table 1. The main constituent elements of the HSWR are S, Cl, P, Na, Mg, Fe, Ca, etc. The content of each metal is very low, indicating that HSWR belongs to non-heavy metal waste slag. In addition, the calorific value of the slag is high, reaching 3,000 cal/g, indicating that this type of slag contains a certain amount of organic substances. The content of heavy metals in the slag is relatively low, indicating that this type of waste residue does not belong to the heavy metal type waste residue.

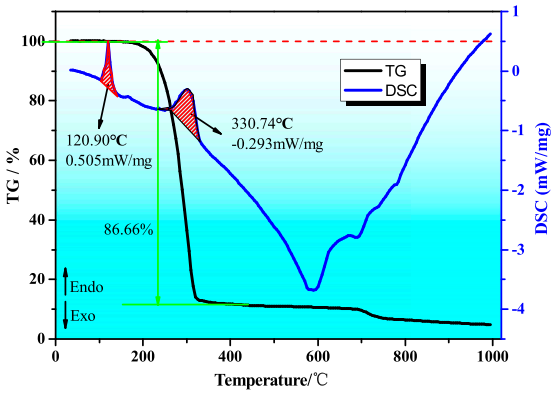

FIGURE 2
TG-DSC curve of HSWR.

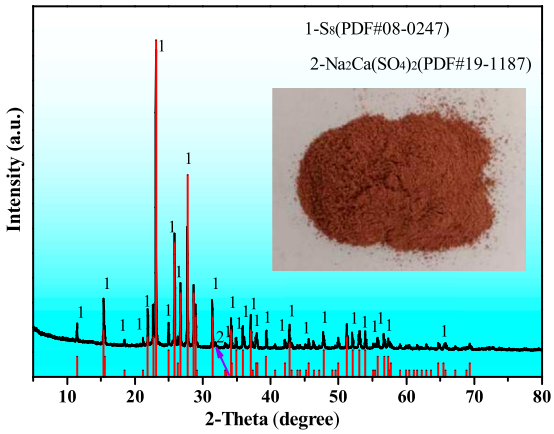

FIGURE 3
XRD pattern of HSWR.

To further determine the composition of organic matter in the slag, the elemental composition of the slag was quantitatively analyzed by EA and chemical quantitative analysis; the results are shown in Table 2. Total sulfur in the HSWR accounts for 72.37%, while the sulfate content only accounts for 2.36%, indicating that the sulfur in the sample slag is not mainly caused by inorganic sulfur-containing compounds. The contents of hydrogen, oxygen and nitrogen are 0.66%, 4.36%, and 2.58%, respectively, which further indicates that most of the sulfur in the slag exists in the form of inorganic sulfur. As shown in Table 1, the chlorine content in the slag is 8.62%, and the content of the chloride phase is 2.57%. It can be speculated that the chlorine in the slag is mainly contained in organic chlorine, with the exception of certain inorganic substances, such as calcium chloride and magnesium chloride. The organic carbon content is directly related to the organic matter content in the slag. Both the total carbon and organic carbon content in the sample slag are 5.96%, indicating that all the carbon in the slag exists in the form of organic matter. The above analysis speculates that the sulfur and chlorine in HSWR slag not only contain sulfate and chloride inorganic substances but also partially contain sulfur-containing (-S-) and chlorine-containing (-Cl-) groups.

3.1.2 Thermal behavior analysis

TG-DSC is usually utilized to reveal the possible reaction trend between two mixtures and the change law of weight and enthalpy value, which is helpful to preliminarily judge the reaction sequence and initial temperature of mixture materials. The TG-DSC analysis results of the HSWR is shown in Figure 2. The sample slag has two obvious endothermic peaks at 120.9 ˚C and 330.74˚C, of which the endothermic peak corresponding to 120.9˚C is mainly attributed to the volatilization of free water, and the endothermic peak at 330.74˚C is mainly attributed to the endothermic volatilization of volatile substances in the slag. The TG curve has a continuous weight loss peak in the range of 157.2˚C–329.4˚C, and the total weight loss reaches 86.66%, indicating that there are numerous volatile substances or easily decomposed substances in the sample residue. It can be speculated that the HSWR is mainly composed of some compounds that are easily decomposed or volatile.

3.1.3 Phase compositions

XRD measurements were collected to analyze the phase composition and crystal phases of sulfur and chlorine in the HSWR. The results are presented in Figure 3. S8 (PDF #08-0247) is the main crystal phase identified in the XRD pattern and has a better crystal form. In addition, a peak corresponding to sulfate also appears at 2θ = 31.9˚. No matching crystal phase related to chlorine element was identified, which may be attributed to the existence of chlorine in the amorphous phase, low chlorine-containing compounds, or the existence of a complex, long-chain, halogenated hydrocarbon phase. However, the bond formation of sulfur and chlorine components in HSWR; the bond structure of organic sulfur, chlorine and carbon; and the number of carbon chains require further analysis.

3.1.4 Micromorphology and microstructure analysis

The microscopic morphology and element distribution of the HSWR sample were analyzed; the results are shown in Figure 4. The microscopic morphology of the HSR sample shows a typical agglomeration phenomenon, with no obvious edges and corners. The structure is dense and shiny; the appearance is similar to a “fungus”; and the particle size distribution is relatively uniform. Mapping results show that the elements Cl, P, O, N, S, and C are distributed in a dispersed type. The purple color representing S is the most obvious, and the distribution is relatively uniform, which further indicates that the sulfur content in the HSWR

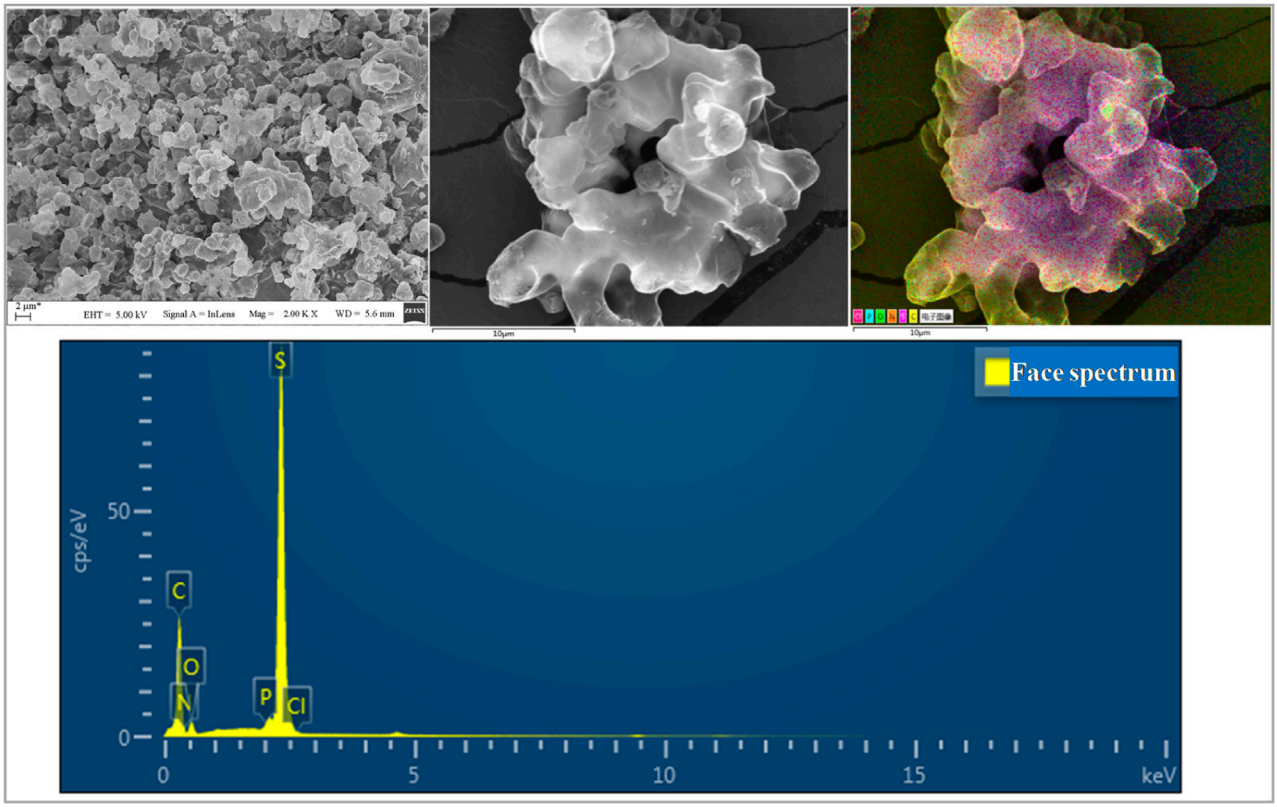

FIGURE 4
Typical SEM-Mapping images of HSWR sample and related EDS results.

is abundant and that the distribution is dispersive. Based on the EDS and mapping data, it can be concluded that the HSWR sample takes sulfur-containing substances as the skeleton, that other inorganic salts are embedded and wrapped in that sulfur-containing substances, and that organic impurities represented by carbon are covered on the surface of the particles.

3.2 Mapping relationship between sulfur and other components

Wang et al. (2015) pointed out that most of the main elements in waste residue have a mapping correlation phenomenon. The main components of HSWR include C, S, Cl, P, Na, Fe, etc., and the sum of their corresponding mass fractions accounts for more than 95% of the waste residue composition. The changes in the component content in the slag will directly affect the bonding and distribution characteristics of sulfur and chlorine. Based on the EDS data (Supplementary Table S1; Supplementary Figure S1, supporting information), the coupling linear mapping relationship between sulfur and other elements is established by using cumulative distribution and linear fitting. According to the results of the linear fitting in Figure 5, the mapping relationships between the six components (C, Na, Cl, P, Si, and Fe) and the sulfur content can be divided into the following three categories:

1) Mapping relationship between C and S (Figure 5A): According to the overall trend analysis, the position with a higher C content has a lower S content, and there is an inverse relationship between the two elements. The slope of the fitting curve of C and S mass content is −1.0326, and the fitting coefficient R^2 is 0.9597, indicating that there is a strong negative tropism between the distribution of S and C. It is speculated that the bond between S and C in HSWR is less likely to form inorganic compounds. However, there is a slight enrichment between C and S in the local area, which may be attributed to the formation of sulfhydryl groups or methylthio groups between organosulfur and organocarbon.
2) Mapping relationship among Cl, P, Na, and S (Figures 5B–D): There is a weak positive correlation between S and the elements Cl, P, and Na, and the curve fitting coefficients are 0.0986, 0.2562, and 0.0385, respectively, indicating that there is a possibility of agglomeration adsorption or bonding

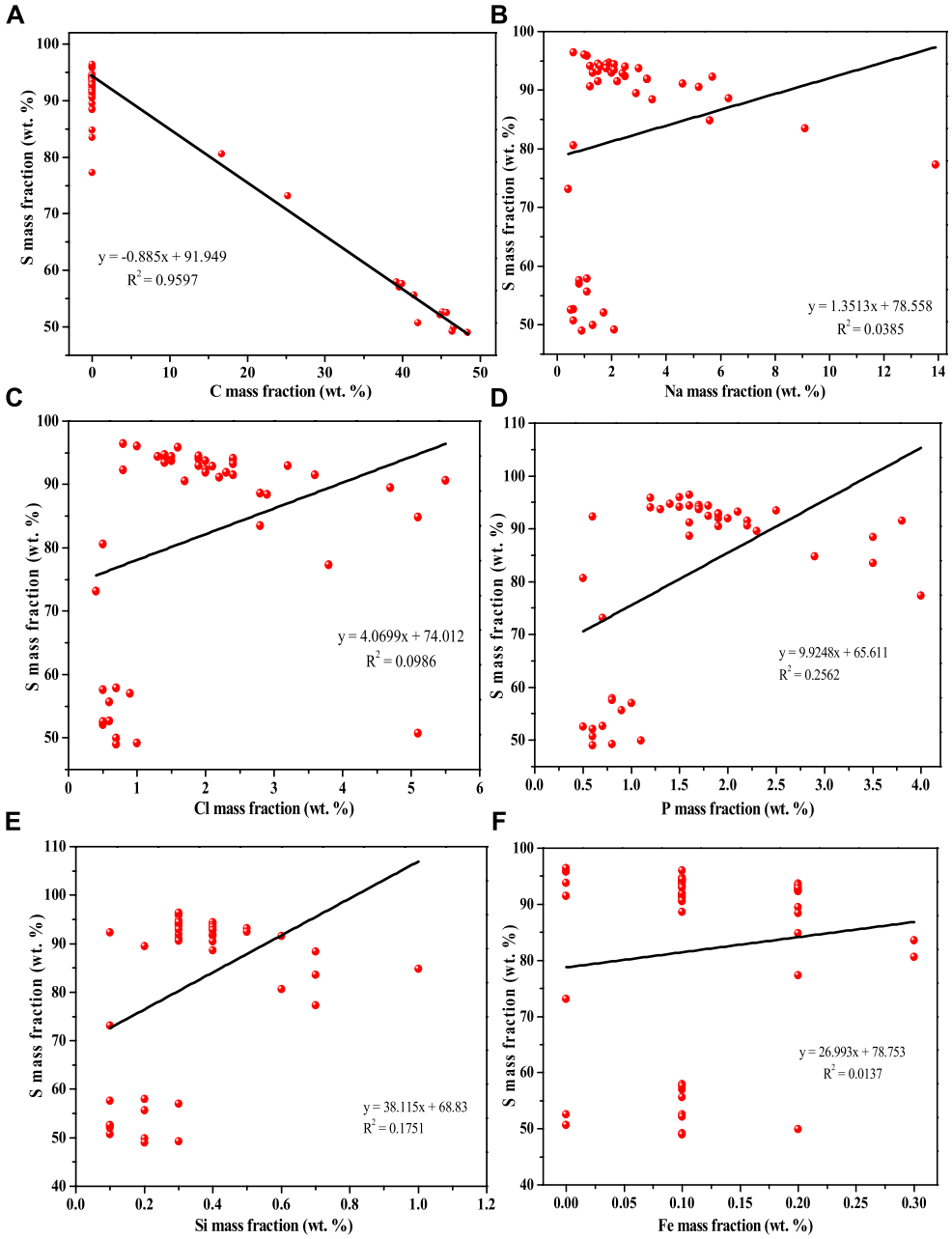

FIGURE 5
Coupling linear mapping relationship between sulfur and other components in HSWR sample.

between S and the elements Cl, P, and Na. In addition, according to the cumulative statistics of element distribution, there is local enrichment of sulfur, that is, in the local area with low Cl, P, and Na contents, the sulfur content can reach approximately 90%, indicating that sulfur basically self-aggregates to form agglomerated sulfur in that area.

3) Mapping relationship among Fe, Si, and S (Figures 5E,F): The linear fitting of the S content and the elements Fe and Si contents in the HSWR is carried out; the fitting coefficients are 0.1751 and 0.0137, respectively. The fitting results show that although there is a weak positive correlation, and both of them belong to both nonaggregated/nonuniform distributions, indicating that there may only be a simple

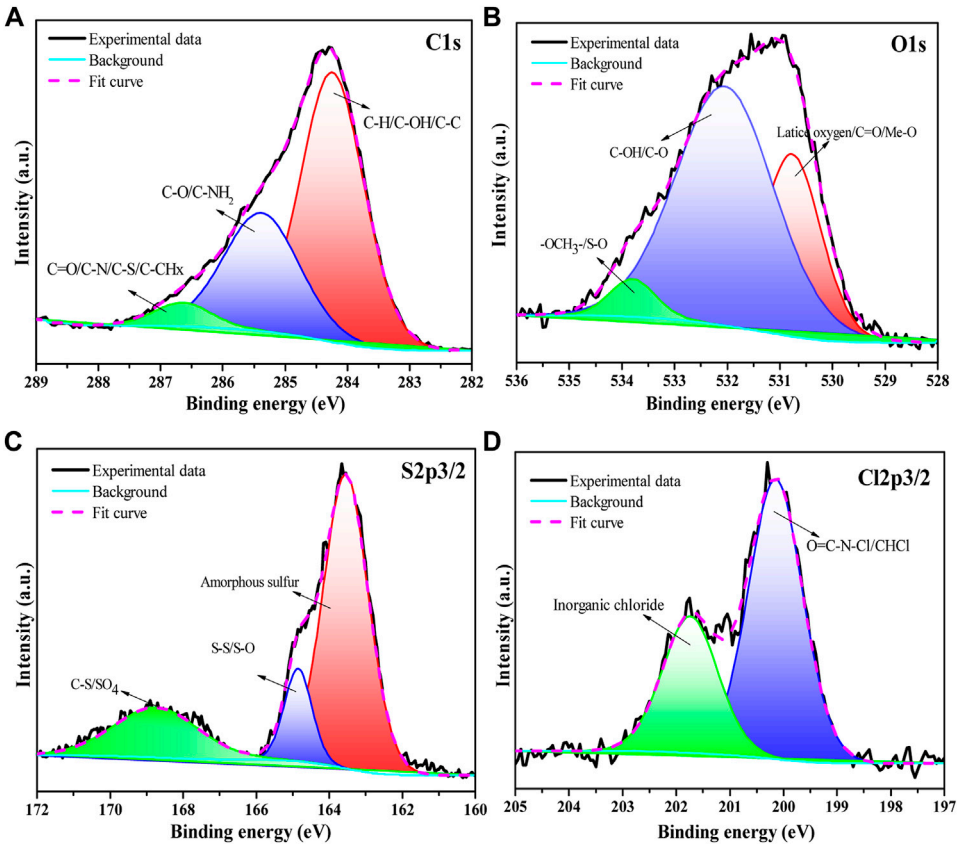

FIGURE 6
Typical deconvoluted peak of HSWR sample. **(A)** C1s, **(B)** O1s, **(C)** S2p3/2, **(D)** Cl2p3/2.

adsorption relationship between S and the elements Fe and Si in the HSWR, and no complex compound is formed.

3.3 Sulfur occurrence state and organic phase in the HSWR

3.3.1 Surface chemical state

XPS was performed to analyze the surface chemical situation of the main elements in the HSWR sample, which was helpful in determining the valence state and occurrence phases of sulfur. The detailed XPS spectra of elements can be classified into two categories, namely, complex chemical states, including O1s and C1s and elements in single chemical states, including Cl2p, S2p, and N1s.

To demonstrate the C-containing compounds in HSWR, the C1s spectrum is deconvolved into three subpeaks at approximately 284.24, 285.38, and 286.65 eV; The results are shown in Figure 6A. The peak at approximately 284.24 eV is most likely due to C-H/C-OH/C–C groups (Cao and Wang, 2017; Zhang et al., 2018), the peak with a binding energy of 285.38 eV is most likely ascribed to C-O/C-NH_2 groups (Yateem, 2019), and the peak located at 286.65 eV is attributed to C=O/C-N/C-S/CH_x (C–C/CH_x/C=C) (Zhang et al., 2018; Li et al., 2019a). The relative contents of the three subpeaks are 62.24%, 32.83%, and 4.94%, respectively (shown in Table 3). The results of the O1s deconvolution peak are shown in Figure 6B, with three subpeaks are fitted at 530.77, 532.04, and 533.8 eV. Among them, 530.77 eV is mainly attributed to the presence of oxygen-containing inorganic salts such as lattice oxygen/C=O/Me-O, for which the relative content is 29.59% (Zhong et al., 2022). The peak corresponding to 532.04 eV is mainly attributed to complex oxygen-containing organic compounds such as C–OH/C–O bonds, with a relative content of 65.65% (Alam et al., 2020). The peak at 284.4 eV mainly corresponds to the–OCH_3-/S-O bonds containing organic sulfur groups (Guo et al., 2010; Emine Sevgili and Karaman, 2019; Mercan and Karaman, 2021). Combined with the results in Table 3, it can be seen that carbon mainly exists as organic carbon chains, such as C-H/C-OH/C–C/C-NH_2 bonds, while oxygen mainly exists as complex oxygen-containing organic compounds and a small amount of oxygen-containing inorganic salts. A small amount of sulfur is linked with carbon and oxygen bonds by sulfhydryl

TABLE 3 Peak positions, FWHM, and relative abundance from curve fitting of C1s and O1s.

	Bonds	Peak (eV)	FWHM	Percentage (%)
C1s	C-H/C-OH/C–C	284.24	1.19	62.24
	C-/C-NH_2	285.38	1.43	32.83
	C=O/C-N/C-S/CH_x	286.65	1.08	4.94
O1s	lattice oxygen/C=O/Me-O	530.77	1.30	29.59
	–OCH_3-/S-O	533.80	1.02	4.76
	C–OH/C–O	532.04	2.20	65.65

TABLE 4 Peak positions, FWHM, and relative abundance from curve fitting of S2p3/2, N1s, and Cl2p3/2.

	Bonds	Peak (eV)	FWHM	Percentage (%)
S2p3/2	Amorphous sulfur	163.54	1.45	66.20
	S-S/S-O	164.85	0.89	12.73
	C-S/SO_4^{2-}	168.75	2.73	21.07
N1s	Sp^2C-N/triazine ring (C–N=C)	398.56	0.98	21.76
	NH_2/pyrrolic NC = N	399.27	1.98	65.92
	C-N-H/–NH/N=N	400.77	2.39	12.31
Cl2p3/2	O=C–N–Cl/CHCl	200.15	1.19	66.75
	Inorganic chloride	201.74	1.22	33.25

groups. Simultaneously, a small amount of sulfur is linked with oxygen and organocarbon bonds by sulfhydryl groups.

According to the results of the typical deconvolution peaks of S2p3/2 (Figure 6C), there are three deconvolution peaks in S2p3/2, of which 163.54 eV mainly corresponds to amorphous sulfur (Zhang et al., 2017b). Combined with the results of Figure 4, it can be seen that this type of sulfur belongs to agglomerated sulfur, for which the relative content reaches 66.20% (Table 4). The binding energy at 164.85 eV is caused by the S–S/S–O bond in crystalline sulfur or sulfur-containing inorganic oxides (Li et al., 2016; Hamisu et al., 2017); the peak at approximately 168.75 eV is assigned to the C-S/SO_4^{2-} bond, which may be caused by the sulfhydryl group or sulfate on the carbon chain (Han et al., 2005). Cl2p3/2 mainly has two deconvolution peaks corresponding to organic chlorine and inorganic compounds (Figure 6D), which are located at 200.15 and 201.74 eV, respectively; their corresponding contents are 66.75% and 33.25% (Table 4), indicating that the chlorine in HSWR mainly exists in the organic state, and some form inorganic chlorides with other metals, such as NaCl, and $CaCl_2$, etc. (Plummer Christopher et al., 2018; Lu et al., 2019).

The N1s spectrum can be deconvoluted into three subpeaks (shown in Figure 7), which correspond to the Sp^2 nitrogen-containing heterocyclic (Sp^2 C-N)/triazine ring (C–N=C) bond (398.56 eV) (Zhao et al., 2012; Zhang et al., 2017a; Li et al., 2019b), NH_2 or NC=N bond in pyrrole (399.27 eV) and C-N-H/–NH/N=N bond (400.77 eV) (Ichrak et al., 2015; Wang et al., 2020; Jta et al., 2021); their contents are 21.76%, 65.92%, and 12.31%, respectively. It can be inferred that nitrogen mainly forms nitrogen-containing heteroatom cyclic organic compounds with carbon and oxygen.

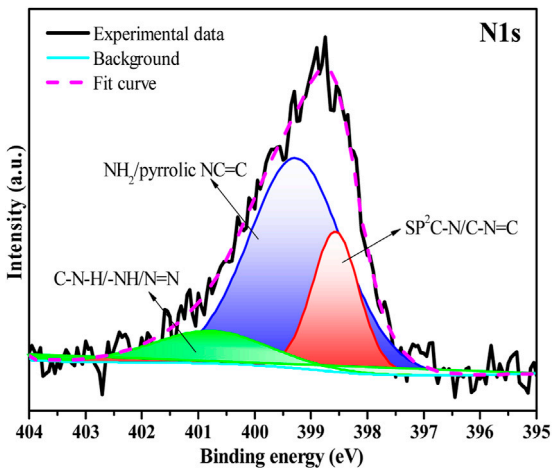

FIGURE 7
The typical deconvoluted peak of N1s spectra.

From the XPS analysis, it can be concluded that most of the sulfur is mainly agglomerated as elemental sulfur and forms the

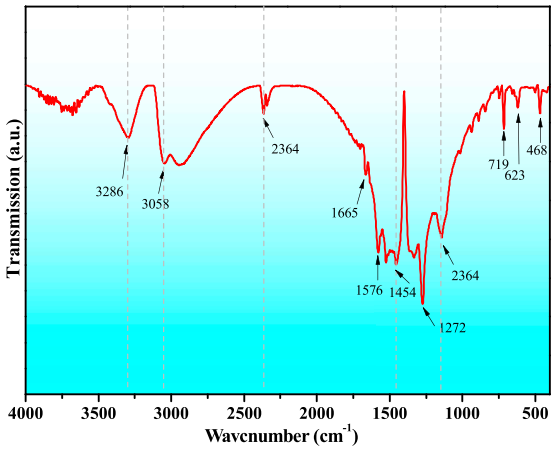

FIGURE 8
FTIR spectra of the HSWR sample.

skeleton of the HSWR sample with some inorganic sulfates and chlorides. Organic compounds with complex aromatic functional groups are formed among C, N, and O and cover the surfaces of solid particles. Organic matter can be combined with some metal cations through functional groups, such as hydroxyl and carbonyl groups, to increase its stability in waste residues.

3.3.2 Sulfur-containing functional group analysis

FTIR was employed to analyze the functional groups present on the surface of the HSWR sample; the results are shown in Figure 8. Many peaks with different degrees of oscillation are distributed at approximately 3,286 cm^{-1}, 3,058 cm^{-1}, 2,364 cm^{-1}, 1,665 cm^{-1}, 1,576 cm^{-1}, 1,272 cm^{-1}, 719 cm^{-1}, and 468 cm^{-1}. The peak located at approximately 3,286 cm^{-1} is mainly related to the stretching vibration of the –OH/CH group (Ahsan and Farooq, 2019), while the peak at 2,364 cm^{-1} is linked to the C-O/C=O stretching vibration in the ketone (Maurer et al., 2014). The stretching vibration peak near 3,058 cm^{-1} is mainly caused by the v (NH)/CH group (Gang and Yuan, 1994). The FTIR wavenumber in the range of 1,576–1,665 cm^{-1} is related to C≡N/C-N groups (Gerber and Erasmus, 2018). The peak at approximately 1,272 cm^{-1} is most likely attributed to the C-O/C-S stretching vibration in the aromatic ring (Poy et al., 2020). The peak located at 719 cm^{-1} is assigned to the stretching vibration of the $-CH_2-/-CONH_2$ group (Bora et al., 2000). According to the literature, sublimated sulfur shows sharp characteristic peaks at 154, 219, and 473 cm^{-1}. Therefore, the peak at 468 cm^{-1} in spectrum of the HSWR sample is mainly caused by the sulfur bond in the agglomerated sulfur. The above FTIR analysis shows that the organic sulfur and chlorine in the slag are connected with the heterocyclic aromatic hydrocarbons through nitrogen methyl, methylene, carbon chain, etc. These organics are deposited on the surface of inorganic agglomerated sulfur and may combine with metal cations through hydroxyl or carboxyl groups, which increases the stability of volatile compounds in the slag and increases the difficulty of removing sulfur and chlorine.

4 Conclusion

The occurrence characteristics of organic components in HSWR from multiple dimensions such as phase composition, chemical situation, and functional groups are researched by combinatorial analysis method. The composition quantitative analysis show that the main constituent elements of the HSWR are S, Cl, P, Na, Mg, Ca, etc. The carbon in the slag basically occurs by organic matter, while the sulfur and chlorine in the slag occur not only in the state of inorganic salts such as sulfate and chloride but also in the form of organics. In addition, the HSWR exhibits significant thermal instability in high temperature, with the maximum weight less of 86.66%. The results of mapping relationship show that in addition to self-aggregation to form agglomerated sulfur, S and C can also form sulfhydryl groups or methylthio groups, but they are unlikely to form inorganic compound bonds. There is a possibility of agglomeration adsorption or bonding between S and the elements Cl, P, and Na, while there may only be a simple adsorption relationship between S and the elements Fe and Si, and the possibility of forming complex compounds is small. Carbon mainly exists in the states of C-H/C-OH/C-C, C-O/C-NH_2, C=O/C-N/C-S/CH_x and constitutes the main chain of the carboxylic ring. Sulfur mainly occurs in three forms, namely, amorphous aggregated sulfur, sulfur-containing inorganic salts such as sulfate, and nitrogen-heterocyclic organic compounds containing sulfhydryl group and methyl sulfur group. These organic compounds constitute branch chains of the organic phase, and combine with metal cations through hydroxyl or carboxyl groups, and deposit on the surface of inorganic agglomerated sulfur. This wrapping structure increases the stability of volatile compounds in the slag and increases the difficulty of sulfur and chlorine removal. Sulfur volatilization and condensation and organic matter cracking and carbonization can be achieved through catalytic pyrolysis-condensation regulation to realize the reduction and harmless treatment of HSWR.

Data availability statement

The original contributions presented in the study are included in the article/Supplementary Material, further inquiries can be directed to the corresponding author.

Author contributions

ZW: Conceived and designed the experiments; contributed on the writing of the manuscript. FJ: Contributed reagents/materials/analysis tools. WL: Analyzed the data. ZZ: Reviewed and revised the manuscript. FN: Analyzed the data. JZ:

Contributed on the writing of the manuscript. WQ and KZ: Performed the experiments.

Acknowledgments

The authors gratefully acknowledge the financial support from the National Natural Science Foundation of China (52064038), the Guangdong Provincial Key Laboratory of R&D for Resource Utilization and Deep Treatment of Hazardous Waste Liquid (2018B030323016). The authors would like to thank from Shiyanjia Lab (www.shiyanjia.com) for the XPS analysis.

Conflict of interest

Authors ZW, WL, ZZ, FN, JZ, WQ, and KZ were employed by the company Dongjiang Environmental Co., Ltd. and FJ was employed by the company Jiangxi Ganchang Evaluation and Testing Technology Consulting Co., Ltd.

Publisher's note

Supplementary material

The Supplementary Material for this article can be found online at: https://www.frontiersin.org/articles/10.3389/fenvs.2022.978559/full#supplementary-material

References

Ahsan, A., and Farooq, M. A. (2019). Therapeutic potential of green synthesized silver nanoparticles loaded PVA hydrogel patches for wound healing. *J. Drug Deliv. Sci. Technol.* 54, 101308. doi:10.1016/j.jddst.2019.101308

Alam, K, Sim, Y, Yu, J-H, Gnanaprakasam, J, Choi, H, Chae, Y., et al. (2020). *In-situ* deposition of graphene oxide catalyst for efficient photoelectrochemical hydrogen evolution reaction using atmospheric plasma. *Mater. (Basel, Switz.* 13, 12–21. doi:10.3390/ma13010012

Bejarano, C. A., Jia, C. Q., and Chung, K. H. (2001). A study on carbothermal reduction of sulfur dioxide to elemental sulfur using oilsands fluid coke. *Environ. Sci. Technol.* 35, 800–804. doi:10.1021/es001581v

Bora, M. M., Dutta, N. N., Tosh, B., and Bhattacharya, K. G. (2000). Reactive extraction of beta-lactam antibiotics: Ir spectroscopic studies. *Chem. Eng. Commun.* 180, 107–126. doi:10.1080/00986440008912204

Cao, J., and Wang, C. (2017). Multifunctional surface modification of silk fabric via graphene oxide repeatedly coating and chemical reduction method. *Appl. Surf. Sci.* 405, 380–388. doi:10.1016/j.apsusc.2017.02.017

Chambers, L. A., and Trudinger, P. A. (1975). Are thiosulfate and trithionate intermediates in dissimilatory sulfate reduction? *J. Bacteriol.* 123, 36–40. doi:10.1128/jb.123.1.36-40.1975

Ciriminna, R., Pagliaro, M., and Luque, R. (2021). Heterogeneous catalysis under flow for the 21st century fine chemical industry. *Green Energy & Environ.* 6, 161–166. doi:10.1016/j.gee.2020.09.013

Ding, X., Li, Q., Wu, D., Liang, Y., Chen, J., Xie, G., et al. (2019). Unexpectedly increased particle emissions from the steel industry determined by wet/semidry/dry flue gas desulfurization technologies. *Environ. Sci. Technol.* 53, 10361–10370. doi:10.1021/acs.est.9b03081

Dong, C, Lu, J, Qiu, B, Shen, B, Xing, M, and Zhang, J. (2018). Developing stretchable and graphene-oxide-based hydrogel for the removal of organic pollutants and metal ions. *Appl. Catal. B Environ.* 222, 146–156. doi:10.1016/j.apcatb.2017.10.011

Egbosiuba, T. C., Abdulkareem, A. S., Kovo, A. S., Afolabi, E. A., and Roos, W. D. (2020). Enhanced adsorption of As(V) and Mn(VII) from industrial wastewater using multi-walled carbon nanotubes and carboxylated multi-walled carbon nanotubes. *Chemosphere* 254, 126780. doi:10.1016/j.chemosphere.2020.126780

Egbosiuba, T. C., Abdulkareem, A. S., Kovo, A. S., Afolabi, E. A., Tijani, J. O., Auta, M., et al. (2020). Ultrasonic enhanced adsorption of methylene blue onto the optimized surface area of activated carbon: Adsorption isotherm, kinetics and thermodynamics. *Chem. Eng. Res. Des.* 153, 315–336. doi:10.1016/j.cherd.2019.10.016

Egbosiuba, T. C., Abdulkareem, A. S., Tijani, J. O., Ani, J. I., Lisak, G., Srinivasan, M., et al. (2020). Taguchi optimization design of diameter-controlled synthesis of multi walled carbon nanotubes for the adsorption of Pb(II) and Ni(II) from chemical industry wastewater. *Chemosphere* 266, 128937. doi:10.1016/j.chemosphere.2020.128937

Egbosiuba, T. C., Egwunyenga, M. C., Tijani, J. O., Mustapha, S., Abdulkareem, A. S., Kovo, A. S., et al. (2022). Activated multi-walled carbon nanotubes decorated with zero valent nickel nanoparticles for arsenic, cadmium and lead adsorption from wastewater in a batch and continuous flow modes. *J. Hazard. Mater.* 423, 126993. doi:10.1016/j.jhazmat.2021.126993

Emine Sevgili, M., and Karaman, M. (2019). Initiated chemical vapor deposition of poly(Hydroxypropyl methacrylate) thin films. *Thin Solid Films* 687, 137446. doi:10.1016/j.tsf.2019.137446

Gang, Z., and Yuan, C. (1994). Synthesis and physicochemical studies on S-methyl-β-N-(ferrocenyl)methylenedithiocarbazate and its rare earth complexes. *Transit. Mater. Chem.* 19, 218–220. doi:10.1007/bf00161894

Gerber, S. J., and Erasmus, E. (2018). Electronic effects of metal hexacyanoferrates: An XPS and FTIR study. *Mater. Chem. Phys.* 203, 73–81. doi:10.1016/j.matchemphys.2017.09.029

Guo, L., Feng, C., Fan, X., Cai, W., and Zhang, J. (2010). S-doped α-Fe_2O_3 as a highly active heterogeneous Fenton-like catalyst towards the degradation of acid orange 7 and phenol. *Appl. Catal. B Environ.* 96, 162–168. doi:10.1016/j.apcatb.2010.02.015

Hamisu, U., Farouk, A., Aziz, A., Raman, W., and Mohd, A. (2017). Surface transformations of TiO_2 anatase deactivated in methylene blue solution with Cl^- ions in the colloid. *J. Taiwan Inst. Chem. Eng.* 80, 203–214. doi:10.1016/j.jtice.2017.06.051

Han, S., Qiu, C., Cheng, X., Ma, S., and Ren, T. (2005). Study of the reasons for discoloration of hydrotreated naphthenic lube base oil under ultraviolet radiation. *Ind. Eng. Chem. Res.* 44, 250–253. doi:10.1021/ie049550m

Huang, X., Yang, J., Wang, J., Bi, J., Xie, C., and Hao, H. (2018). Design and synthesis of core–shell Fe3O4@PTMT composite magnetic microspheres for adsorption of heavy metals from high salinity wastewater. *Chemosphere* 206, 513–521. doi:10.1016/j.chemosphere.2018.04.184

Ichrak, L., Patrice, M., and Bruno, C. (2015). Copper (II) ions adsorption from aqueous solutions using electrospun chitosan/peo nanofibres: Effects of process variables and process optimization - ScienceDirect. *J. Water Process Eng.* 7, 295–305.

Jta, B., Yca, B., Swa, B., and Lza, B. (2021). Engineering of UiO-66-NH_2 as selective and reusable adsorbent to enhance the removal of Au(III) from water: Kinetics, isotherm and thermodynamics. *J. Colloid Interface Sci.* 601, 272-282. doi:10.1016/j.jcis.2021.05.121

Kline, M. A., Barley, M. H., and Meyer, T. J. (1987). Electrocatalytic reduction of bisulfite to hydrogen sulfide based on a water-soluble iron porphyrin. *Inorg. Chem.* 26, 2196–2197. doi:10.1021/ic00261a005

Li, B., Guo, J., Lv, K., and Fan, J. (2019). Adsorption of methylene blue and Cd(II) onto maleylated modified hydrochar from water. *Environ. Pollut.* 254, 113014. doi:10.1016/j.envpol.2019.113014

Li, H., Wang, Z., Zhang, Y., Wang, X., Yin, F., Maximov, M. Y., et al. (2016). Interconnected nitrogen-doped carbon nanofibers derived from polypyrrole for high-performance Li/S batteries. *Russ. J. Appl. Chem.* 89, 1336–1340. doi:10.1134/s107042721608019x

Li, X., Han, J., Liu, Y., Dou, Z., and Zhang, T. A. (2022). Summary of research progress on industrial flue gas desulfurization technology. *Sep. Purif. Technol.* 281. doi:10.1016/j.seppur.2021.119849

Li, Z., Dong, W., Du, X., Wen, G., and Fan, X. (2019). A novel photoelectrochemical sensor based on g-C_3N_4@CdS QDs for sensitive detection of Hg^{2+}. *Microchem. J.* 152, 104259. doi:10.1016/j.microc.2019.104259

Liu, F., Cai, M., Liu, X., Zhu, T., and Zou, Y. (2021). O_3 oxidation combined with semi-dry method for simultaneous desulfurization and denitrification of sintering/pelletizing flue gas. *J. Environ. Sci.* 104, 253–263. doi:10.1016/j.jes.2020.11.021

Liu, Z., Wang, G., Li, P., and Li, C. (2019). Investigation on combustion of high-sulfur coal catalyzed with industrial waste slags. *J. Energy Inst.* 92, 621–629. doi:10.1016/j.joei.2018.03.010

Lu, W., Yi, Y., Ning, C., Ge, M., and Jahangir, A. (2019). Chlorination treatment of meta-aramid fibrids and its effects on mechanical properties of polytetramethylene ether glycol/toluene diisocyanate (PTMEG/TDI)-Based polyurethane composites. *Polymers* 11, 1794–1806. doi:10.3390/polym11111794

Maurer, L. M., Tooker, C. A., and Felix, H. S. (2014). Characterization of polyimide via FTIR analysis. *J. Appl. Phys.* 83, 7813–7821.

Mentzen, B. F., Bergeret, G., Emerich, H., and Weber, H. P. (2010). Reactive intermediates of the reduction of SO_2 on activated carbon. *J. Phys. Org. Chem.* 16, 824–830.

Mercan, E. S., and Karaman, M. (2021). Coating of hydrophilic poly(hydroxypropyl methacrylate) thin films via pulsed-initiated chemical vapor deposition method. *J. Coat. Technol. Res.* 18, 1261–1268. doi:10.1007/s11998-021-00486-w

Plummer Christopher, M., Zhou, Houbo, Zhu, Wen, Huang, Huahua, Lixin, L., and Chen, Y. (2018). Mild halogenation of polyolefins using an N-haloamide reagent. *Polym. Chem.* 9, 1309–1317. doi:10.1039/c8py00013a

Poy, S. Y., Bashir, S., Omar, F. S., Saidi, N. M., Ramesh, S., Sundararajan, V., et al. (2020). Poly (1-vinylpyrrolidone-co-vinyl acetate) (PVP-co-VAc) based gel polymer electrolytes for electric double layer capacitors (EDLC). *J. Polym. Res.* 27, 50–58. doi:10.1007/s10965-020-2016-x

Raymundo-Pinero, E., Cazorla-Amorós, D., Lecea, S. M. D., and Linares-Solano, A. (2000). Factors controling the SO_2 removal by porous carbons: Relevance of the SO_2 oxidation step. *Carbon N. Y.* 38, 335–344. doi:10.1016/s0008-6223(99)00109-8

Tang, H., Xu, M., Hu, H., Yang, F., Yang, Y., Liu, H., et al. (2018). *In-situ* removal of sulfur from high sulfur solid waste during molten salt pyrolysis. *Fuel* 231, 489–494. doi:10.1016/j.fuel.2018.05.123

Tceab, C., and Asab, C. (2021). Highly efficient as-synthesized and oxidized multi-walled carbon nanotubes for copper(II) andzinc(II) ion adsorption in a batch and fixed-bed process. *J. Mater. Res. Technol.* 15, 2848–2872. doi:10.1016/j.jmrt.2021.09.094

Tolmachev, Y. V., and Scherson, D. A. (1999). Electrochemical reduction of bisulfite in mildly acidic buffers: Kinetics of sulfur DioxideBisulfite interconversion. *J. Phys. Chem. A* 103, 1572–1578. doi:10.1021/jp983752c

Vásquez-Céspedes, S., Betori, R. C., Cismesia, M. A., Kirsch, J. K., and Yang, Q. (2021). Heterogeneous catalysis for cross-coupling reactions: An underutilized powerful and sustainable tool in the fine chemical industry? *Org. Process Res. Dev.* 25, 740–753. doi:10.1021/acs.oprd.1c00041

Wang, Q., Guo, X., Tian, Q., Liao, L., and Yongzhu, Z. (2015). Multicomponent slag-forming behavior and slag shape optimization in oxygen bottom-blown copper smelting slag. *Chin. J. Nonferrous Metals* 25, 1678–1686.

Wang, S., Liu, J., Huang, Y., and Yang, N. (2020). Selective sensing of Mn2+ based on ZnCdS/ZnS QD/carboxymethyl chitosan/g-C3N4 nanosheet nanocomposite film by the conformational regulation of polymer chain. *Appl. Surf. Sci.* 530, 147255. doi:10.1016/j.apsusc.2020.147255

Wang, Z., Xu, W., Jie, F., Zhao, Z., and Liu, H. (2021). The selective adsorption performance and mechanism of multiwall magnetic carbon nanotubes for heavy metals in wastewater. *Sci. Rep.* 11, 16878–8. doi:10.1038/s41598-021-96465-7

Wang, Z., Xu, W., Li, Y., Zhao, Z., Wang, Y., Zeng, G., et al. (2022). Diffusion behaviors and mechanism of copper-containing sulfide in fayalite-type slag: A key step of achieving copper slag depletion. *Colloids Surfaces A Physicochem. Eng. Aspects* 638, 128264. doi:10.1016/j.colsurfa.2022.128264

Wang, Z., Zhao, Z., Zhang, L., Liu, F., Peng, B., Chai, L., et al. (2019). Formation mechanism of zinc-doped fayalite ($Fe_{2-x}Zn_xSiO_4$) slag during copper smelting. *J. Hazard. Mater.* 364, 488–498. doi:10.1016/j.jhazmat.2018.10.071

Yao, J., Yang, L., Ye, Z., Wang, J., Li, Y., and Tong, X. (2019). Process optimization of industrial waste salts separated into acid/base for the realization of resource utilization by bipolar membrane electrodialysis. *Desalination Water Treat.* 172, 377–385. doi:10.5004/dwt.2019.24603

Yateem, A. H. (2019). Rotational barrier and conjugation: Theoretical study of resonance stabilization of various substituents for the donors NH_2 and OCH_3 in substituted 1, 3-butadienes. *Indones. J. Chem.* 19, 1055–1065. doi:10.22146/ijc.42850

Zhang, C., Chen, Z., Guo, W., and Zhu Chengwu, Y. (2018). Simple fabrication of Chitosan/Graphene nanoplates composite spheres for efficient adsorption of acid dyes from aqueous solution. *Int. J. Biol. Macromol.* 112, 1048–1054. doi:10.1016/j.ijbiomac.2018.02.074

Zhang, J., Lv, J., Kai, D., Qi, L., and Zhu, G. (2017). Facile and green synthesis of novel porous g-C_3N_4/Ag_3PO_4 composite with enhanced visible light photocatalysis. *Ceram. Int.* 43, 1522–1529. doi:10.1016/j.ceramint.2016.10.125

Zhang, Y., Dong, K., Zheng, L., Wang, H., Ma, S., Zhang, A., et al. (2017). Sulfurized hematite for photo-Fenton catalysis. *Prog. Nat. Sci. Mater. Int.* 4, 443–451. doi:10.1016/j.pnsc.2017.08.006

Zhao, M. L., Li, D. J., Gu, H. Q., Guo, M. X., and Zhang, Y. T. (2012). Vitro cell adhesion and hemocompatibility of carbon nanotubes with CNx coating. *Curr. Nanosci.* 8, 451–457.

Zhao, Y., Zhuang, X., Ahmad, S., Sung, S., and Ni, S.-Q. (2020). Biotreatment of high-salinity wastewater: Current methods and future directions. *World J. Microbiol. Biotechnol.* 36, 37. doi:10.1007/s11274-020-02815-4

Zhao, Z., Xu, W., Wang, Z., Qin, W., Lei, J., Guo, X., et al. (2021). Investigation of organic impurity and its occurrence in industrial waste salt produced by physicochemical process. *PLoS ONE* 8, e0256101–14. doi:10.1371/journal.pone.0256101

Zhong, W. M., Liu, Q. X., Jiang, Y. P., Deng, M. L., Li, W. P., and Tang, X. G. (2022). Ultra-high dielectric tuning performance and double-set resistive switching effect achieved on the Bi 2 NiMnO 6 thin film prepared by sol-gel method. *J. Colloid Interface Sci.* 606, 913–919. doi:10.1016/j.jcis.2021.08.109

Zilberchmidt, M., Shpirt, M., Komnitsas, K., and Paspaliaris, I. (2004). Feasibility of thermal treatment of high sulfur coal wastes. *Miner. Eng.* 17, 175–182. doi:10.1016/j.mineng.2003.10.026